Ranking and categorizing large-scale saline aquifer formations based on optimized CO2 storage potentials and economic...

Article *in* International Journal of Greenhouse Gas Control · July 2017

CITATIONS
0

READS
7

4 authors, including:

Rebecca D Allen
SINTEF
10 PUBLICATIONS **4** CITATIONS
SEE PROFILE

Halvor Nilsen
SINTEF
63 PUBLICATIONS **653** CITATIONS
SEE PROFILE

Knut-Andreas Lie
SINTEF Digital, Oslo, Norway
159 PUBLICATIONS **2,434** CITATIONS
SEE PROFILE

Ranking and categorizing large-scale saline aquifer formations based on optimized CO_2 storage potentials and economic factors

Rebecca Allen[a,*], Halvor M. Nilsen[a], Odd Andersen[a], Knut-Andreas Lie[a]

[a]*SINTEF Digital, Mathematics and Cybernetics, PB 124 Blindern, 0314 Oslo, Norway*

Abstract

The process of selecting a CO_2 storage site involves evaluating many potentially suitable sites in terms of their storage potentials as well as their associated technical and economic limitations. As such, it is useful to apply a ranking scheme that makes use of several different criteria and weights each criterion based on its relative importance in the overall evaluation. In this study, we demonstrate one such possible ranking workflow using real formation datasets from CO_2 Storage Atlas of the Norwegian Continental Shelf. The workflow involves computing practical storage potentials using a generic well placement scheme, mathematical optimization and vertical-equilibrium modeling, and is general in the sense that it can be applied to other formation datasets. Economic factors related to the transportation and injection of CO_2 are represented by the number of injection wells required, depth of injection, and distance from a CO_2 point source. The purpose of this study is not to provide formation-specific capacity estimates or efficiency factors for engineering purposes, due to the simplifying assumptions used in this work, and the fact that our specific datasets come with their own limitations (i.e., homogeneous rock properties, lack of fault data). Rather, the purpose is to demonstrate a general ranking scheme that reflects operational limitations and the economic factors likely to be involved in any commercial or demonstration CCUS project.

Keywords: Formation ranking, Storage potentials, Economic factors, Optimization, Vertical-Equilibrium simulation, Storage Atlas

1. Introduction

Geological CO_2 storage is considered a promising strategy to reduce the earth's annual greenhouse gas emissions. Both commercial and demonstration projects are in operation today. The longest running is the Sleipner project, which has successfully stored 16 Mt since its commencement two decades ago. However, to make a significant reduction in CO_2 emissions, one would globally need to inject on the order of gigatonnes per year. This would require large-scale injection of CO_2 in many saline aquifers and depleted oil fields located around the world. This will require a systematic approach to evaluating such aquifers and reservoirs in terms of their suitability and capacity for storage [1].

Indeed, efforts have been made to develop methods of evaluating a particular set of saline aquifers and/or oil reservoirs, e.g., in the USA [2], Canada [3], Australia [4], South Africa [5], Ireland [6], the UK [7, 8], the Netherlands [9], and Nordic regions [10, 11, 12, 13, 14]. These evaluation methods make use of quantitative criteria such as storage potentials, reservoir and sealing properties, proximity to CO_2 point sources, and storage costs, while others include qualitative measures such as leakage risk, safety, and data coverage. Out of the quantitative criteria, estimation of storage potentials often receives the most attention and a wealth of literature is available on the subject, e.g., [15]. Efforts have been made to develop a storage cost model that accounts for injection costs, costs to comply with various regulations (e.g., well, monitoring, etc.), taxes, and financing costs [16, 17]. Despite this, detailed economics are commonly neglected in atlas inventories or ranking schemes and is perhaps the most ambiguous of the above mentioned criteria.

Storage potentials are typically computed statically using a volumetric approach, which is the simplest and most basic capacity estimation. This approach applies a storage efficiency factor S_{eff} to the formation's pore volume deemed suitable for storage V_p, to compute the storable mass, i.e.,

$$M_{co2} = S_{\text{eff}} \rho_{co2} V_p, \tag{1}$$

*Corresponding author.

Email addresses: Rebecca.Allen@sintef.no (Rebecca Allen), HalvorMoll.Nilsen@sintef.no (Halvor M. Nilsen), Odd.Andersen@sintef.no (Odd Andersen), KnutAndreas.Lie@sintef.no (Knut-Andreas Lie)

where ρ_{co2} is the CO_2 density at reservoir conditions, and M_{co2} is storage potential in terms of CO_2 mass [10]. The pore volume deemed suitable for storage is computed by $V_p = V\phi NTG$, where V is the total (or gross) volume (i.e., rock and solid combined), ϕ is porosity, and NTG is the net-to-gross ratio. We note that the net-to-gross ratio is sometimes neglected in volumetric estimates, and that the total volume V is calculated using an average aquifer thickness and aquifer area, e.g., [15, 2]. The storage efficiency factor is typically determined by the degree to which the formation is in communication with neighboring formations; an "open" or "closed" formation refers to whether or not fluid is able to be transmitted in or out of the formation. The range of factors reported in literature is 1.5–3.6% for open systems, and 0.3–1.2% for closed systems [18]. These values come from combining geological and laboratory measurements, past experience, and statistical techniques based on simplifying assumptions about the injection process. While the approach of combining volumetric data and efficiency factors is useful in the production of regional or national storage inventories, it does not capture temporal aspects of other practical legal or economic constraints that will most likely dictate realistic storage strategies.

Representation of storage costs have been included in some of the evaluation methods. In Bachu [1] and Bachu [19], a weighted normalized parametric procedure was used to rank the suitability of sedimentary basins and oil reservoirs for CO_2 storage and/or CO_2–EOR, respectively. The weighting was applied to three parameters: reservoir storage capacity, distance from CO_2 source and storage site, and depth of storage site. These parameters reflect the economics involved in a CCUS project, which includes costs related to capture, transportation, and injection, as well as money saved due to storage (e.g., carbon credits, avoid paying CO_2 emission tax, benefit to environment, etc.). Similarly, Ramírez et al. [9] used a weighting approach to screen and rank formations based on various criteria, which included storage costs. The storage costs were broken down into number of wells required, site development, surface facilities, monitoring, and operation and maintenance. They used the storage capacity and an assumed injection rate to determine the number of wells required per site.

In this work, we demonstrate a ranking workflow that attempts to reflect the practical, technical, and economical requirements of CO_2 storage projects in saline aquifer. To do this, we use storage potentials that were computed using simulation and mathematical optimization, and account for project costs related to wells and transportation. This ranking workflow makes use of the weighted normalized parametric procedure presented in Bachu [1] and Bachu [19], which was applied to sedimentary basins in Canada and oil reservoirs in Alberta, respectively. Here, we apply the ranking workflow to geomodels of large-scale saline aquifers located along the Norwegian Continental Shelf, which are publicly available from the Norwegian Petroleum Directorate (NPD) [10]. Our demonstrated ranking workflow is flexible in that it is not limited to just the criteria used in this work. Other quantitative and/or qualitative aspects can be included into the scheme if deemed necessary.

2. Methods

Our ranking procedure includes the calculation of optimized CO_2 storage potentials, and economic factors related to cost of transport and injection of CO_2 from point sources. Fig. 1 illustrates the workflow of obtaining the storage potentials and their categorization in terms of what limited the injection of more CO_2. Each part of this workflow, as well as the final ranking procedure, is explained in this section.

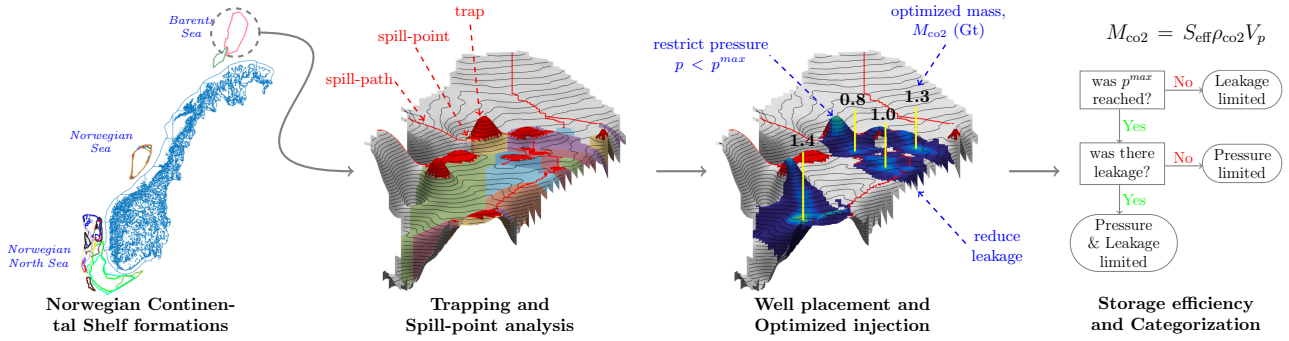

Figure 1: Workflow of obtaining a formation's optimized storage potential (or storage efficiency), and categorizing it in terms of what limited the injection of more CO_2. "Leakage-limited" means that storage potential was limited due to CO_2 flowing out from the aquifer's open boundaries and into an adjacent aquifer (not leakage through the caprock or wells). "Pressure-limited" means that storage potential was limited due to pressure buildup, which reached a certain fraction of the overburden pressure somewhere within the aquifer (not necessarily at the well).

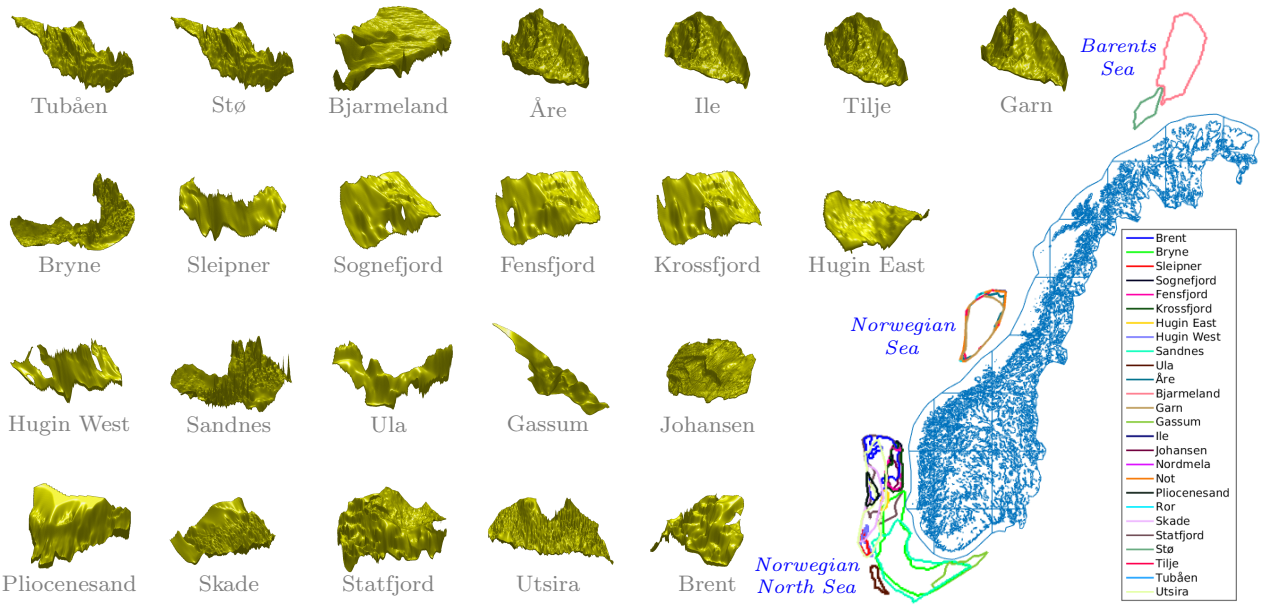

Figure 2: Norwegian Continental Shelf formations suitable for CO_2 storage according to the Norwegian Petroleum Directorate (NPD). Datasets are publicly-available from the NPD. *Map on right*: Approximate location of the formations along the Norwegian Continental Shelf (including a few sealing formations, i.e., Not, Ror, Nordmela, which are not investigated in this study due to lack of storage potential). *Individual formation plots*: 3D view of each formation constructed from its dataset (with z-scale exaggerated to emphasize the unique caprock topography of each formation).

2.1. Formation datasets & volumetric capacities

Our ranking method is demonstrated using 23 subsea geological formations located along the Norwegian Continental Shelf, that have been considered as potential candidates for CO_2 storage; see Fig. 2. These formations are part of NPD's publicly available CO_2 Storage Atlas [10]. For simplicity, we treat each formation as a separate unit. Based on our construction of each dataset, and applying the same storage efficiency values used in Halland et al. [10], our computed volumetric capacities are presented in Table 1. In addition, we tabulate other averaged data including formation caprock depth, total (or gross) rock volume, porosity, net-to-gross ratios (if available), and CO_2 density. Unlike in previous work (i.e., [10, 11]), we consider the entire aquifer volume and calculate CO_2 density based on pressure and temperature as a function of depth, as opposed to a constant, fixed value. More specifically, pressure is assumed to be hydrostatic, and temperature is found by using the temperature gradient, seafloor temperature, and seafloor depth. These required inputs were referenced from the Atlas or other sources, or assumed if data was missing; see Table A.3. Due to these differences, it is not surprising that our volumetric capacity estimates in Table 1 differ from those given in the NPD Storage Atlas [10].

2.2. Optimized dynamic storage potentials

While the volumetric capacities presented above are based on aquifer pore volume, capacity estimates can also be obtained based on the injection and migration of CO_2 within an aquifer. Such estimates are typically called *dynamic* capacities, and better represent practical or achievable storage potentials. In our ranking methodology, we estimate capacities using a generic well placement scheme, mathematical optimization, and vertical-equilibrium simulation. To summarize, we place wells somewhere in the aquifer based on the trapping structure of the top surface and assign the wells with an initial injection rate. These initial rates are based on the upslope structural-trapping capacity from each well. Then, we optimize the injection rates according to an objective function that penalizes aquifer leakage and pressure buildup. Aquifer leakage and pressure buildup is determined using simulation of the injection and long-term migration of CO_2. Since we are capturing the dynamics of the system, in addition to optimizing the injection rates according to our objective (i.e., maximize storage while minimizing leakage and pressure buildup), we call this estimate an "*optimized dynamic*" storage potential (optimized storage potential for short). We emphasize that this approach is general in the sense that it can be applied to other formation datasets. The following paragraphs explain this part of the workflow in more detail.

The strategy behind the generic well placement scheme is to position CO_2 injection wells so as to exploit as much of the aquifer's trapping capacity as possible, and with as few wells as possible. We consider it natural

Table 1: Formation properties and associated volumetric storage capacities. '-' denotes data not available. Grids un-coarsened. z_t denotes average depth of top surface, V is total formation volume (rock and fluid), ϕ is porosity, NTG is average net-to-gross ratio, ρ_g is average CO_2 density at reservoir conditions, S is storage efficiency factor given by NPD [10], and M is storage capacity computed by (1).

Formation	Sea	z_t (m)	V (Gm^3)	ϕ	NTG	ρ_g (kg/m^3)	S (%)	M (Gt)
Tubåen	Barents	2486	431	0.15	0.65	665	3.0	0.741
Stø	Barents	2339	449	0.16	0.84	670	3.0	1.136
Bjarmeland	Barents	996	1431	0.20	0.95	786	3.0	6.332
Are	Norwegian	2223	5319	0.21	0.30	601	0.7	1.406
Ile	Norwegian	1891	1166	0.27	0.25	612	0.2	0.096
Garn	Norwegian	1668	2682	0.27	0.25	622	0.2	0.225
Tilje	Norwegian	2080	3230	0.21	0.30	606	0.7	0.863
Brent	North	3454	3462	-	-	621	-	-
Bryne	North	2382	4429	0.13	1.00	625	4.5	15.944
Sleipner	North	3244	281	-	-	621	-	-
Sognefjord	North	1952	906	0.19	1.00	631	5.5	6.136
Fensfjord	North	1952	965	0.19	1.00	631	5.5	6.527
Krossfjord	North	1976	786	0.19	1.00	631	5.5	5.327
Hugin East	North	2705	93	0.13	1.00	623	5.5	0.398
Hugin West	North	3224	378	0.13	1.00	621	5.5	1.616
Sandnes	North	2043	1546	0.09	1.00	628	4.5	3.820
Ula	North	3437	399	0.18	1.00	620	-	-
Gassum	North	1790	631	0.12	1.00	572	5.5	2.288
Johansen	North	2484	343	0.20	1.00	625	3.0	1.286
Pliocenesand	North	368	296	-	-	94	-	-
Skade	North	840	2356	0.21	1.00	556	4.0	8.748
Statfjord	North	3672	4184	0.11	1.00	620	4.5	12.485
Utsira	North	782	3874	0.21	1.00	520	4.0	15.761

to position the wells based on the location and capacity of the structural traps found in the top surface. This of course does not mean we are only interested in exploiting the structural trapping capacity. We recognize that other forms of trapping will take place as the CO_2 plume migrates throughout the aquifer, however this migration will largely be dictated by the trapping structure. The trapping structure includes the location of the structural traps, the catchment regions associated with each structural trap, and the connection or "spill-path" between each trap (i.e., the path that buoyancy-driven CO_2 is likely to take as it spills from one trap to another). By placing a well downslope from a spill-path containing several traps, the injected CO_2 will eventually migrate upslope and fill the traps along it pathway (in addition to becoming trapped by other forms). This is the basic idea behind the well placement algorithm which we use in this work, which has been referred to as a *greedy* algorithm in previous work; see Nilsen et al. [20] and Lie et al. [21]. The trapping structure is precomputed using a spill-point analysis, and wells are placed according to the best available, reachable structural-trapping capacity. To exploit as much trapping as possible, wells are placed at the deepest elevation within a given catchment region while respecting certain *buffer* distances to various boundaries. These buffers are the minimum distances that can exist between a well and the aquifer boundary. Wells are placed until either the next well's injection mass is less than 1% of the total structural capacity, or until the entire trapping structure has been assessed. In this work, we employ a slightly modified approach to the greedy algorithm that places a set of wells directly in specific catchment regions. This is useful if a spill-path contains a trap with a relatively large trapping capacity, which would be difficult to exploit with only one well, especially a well located very far downslope from the trap.

Fig. A.10 illustrates the well locations and the initially injected masses as suggested by the modified greedy algorithm. The corresponding mass injection rates are simply calculated by dividing these injected masses by the injection period (i.e., 10Mt/10years = 1Mt/year). Various buffer distances were used to place these wells, and are reported in Table A.4. These distances were chosen based on judgment (e.g., a well with a high injection rate should be placed farther from the aquifer boundary to minimize leakage). To reduce computing time required for simulations, most grids were coarsened by specific factors that were chosen such that the main structural traps would still be captured. Some grids were not coarsened since they were already comprised of a relatively small number of grid cells.

The initial injection rates of the wells are computed based on the structural-trapping capacity upslope from the wells only. However, since other forms of trapping will take place as CO_2 migrates through the aquifer, these rates are not necessarily optimal and may be too low. On the other hand, since our objective is to minimize excess leakage and preserve caprock integrity, some of these rates may be too high. As such, an optimal injection

strategy can be found according to the following objective function:

$$J = M_I - C_L M_L - C_P \sum_i^N \left(\max(0, p_i - p_i^{\lim})\right)^2 . \tag{2}$$

where J can be thought of as the credited CO_2 mass stored, M_I is the amount injected, M_L is the amount leaked by the end of the simulated migration period or that is forecast to leak by time infinity, p_i is the cell pressure, and $p_i^{\lim}$ is the cell's predefined pressure target. The term C_L is a unitless factor that penalizes leakage. It can be interpreted as a ratio between the cost of leaking and the CO_2 tax credit per mass stored. The term C_P is a pure penalization factor used in the algorithm to avoid overpressure, with units of mass per pressure squared. Here, we use the term *leakage* to refer to CO_2 that exits the model domain through any open, lateral boundaries (i.e., we do not model CO_2 leakage through the relatively impermeable caprock). While capacity estimation typically does not account for CO_2 leakage, the rationale for maximizing storage while penalizing leakage is that more CO_2 could be injected and trapped in the aquifer if a small amount of leakage (i.e., waste) was permitted.

As introduced, the factors C_L and C_P act to constrain (via penalization) CO_2 leakage and pressure buildup, respectively. Here, C_L is user defined (herein, 5) such that $1/C_L$ is the fraction of the injected mass that is allowed to leak according to political or technical requirements. Penalizing pressure is more complicated, in that the user cannot chose C_P directly. Instead, the user selects a target on the maximum pressure and a tolerance (herein, 2%) by which we are allowed to exceed this target. The factor C_P is iteratively increased until we converge within this tolerance to approximate the constraint. The starting value of C_P is chosen such that the pressure term in (2) is negligible compared to the first two terms, $M_I - C_L M_L$. The pressure target $p^{\lim}$ is assumed to be 90% of the overburden pressure, as suggested in Nordbotten and Celia [22]. This pressure target does not necessarily reflect the actual fracture pressures of our formations, and may be considered too high for regulatory purposes; therefore, in this work we use this target for illustrative purposes only. The overburden pressure is computed to be the weight of all fluid or media layers (i.e., sea and saturated sandstone) lying above the saline aquifer's caprock, and thus the pressure target is computed by

$$p^{\lim} = 0.9 \times \left(p_s + \int_{z_s}^{z_t} (\phi \rho_f + (1-\phi)\rho_s) g_z dz \right), \tag{3}$$

where ρ_f and ρ_s are the fluid and solid densities respectively, ϕ is porosity, and p_s is surface pressure; see Nordbotten and Celia [22] for details. The integral is taken vertically from the depth of the sea surface $z_s = 0$ to the depth of the formation caprock z_t, which includes a layer of sea water, and a layer of geological media between the sea bottom and formation caprock. We assume a surface pressure of 1 atmosphere, and a sea water density of 1000 kg/m^3. In lack of actual information, we assume that the media above the formation is comprised of the same type of fluid and rock as in the formation, thus we set this layer's porosity equal to the average of the formation porosity, and the fluid density equal to the formation's initial fluid density. We also assume a rock density of 2000 kg/m^3 as a conservative dry bulk density of sandstone.

To find the global maximum of (2), we use the Broyden–Fletcher–Goldfarb–Shanno (BFGS) algorithm, using Wolfe conditions [23, 24] with an inexact cubic line-search based on values and derivatives. The state variables (i.e., CO_2 saturation and pressure) that are required to evaluate (2) are determined via simulation. In (2), the amount leaked is equal to the difference between the amount injected and the amount stored, where the amount stored is based on CO_2 density and the simulated CO_2 saturations. These saturations are never greater than 1 minus the residual water saturation. The derivatives (with respect to the state variables) are calculated using the adjoint method; see Jansen [25]. While many simulations are required to find the global maximum of (2), the use of vertical-equilibrium (VE) modeling [22, 26, 27] makes the simulations rapid and thus the CPU time is manageable. The underlying assumptions of VE modeling are valid for the flow dynamics of our problem: CO_2 and the formation fluid segregate into vertical layers once CO_2 is injected into the formation, due to the density difference between the fluids. Since the lateral migration of CO_2 compared to its vertical flow is orders of magnitude larger, this vertical segregation is assumed to occur instantaneously. As such, the fluid flow equations can be vertically integrated and solved using a 2D grid, which drastically reduces the computational cost of solving a 3D model. Once the 2D equations are solved, the vertical distribution of CO_2 (in terms of its trapping mechanisms) are reconstructed by analytical expressions.

Once the optimized injection rates have been found by maximizing (2), the optimized storage potential s is the amount of CO_2 that is forecast to remain within the aquifer. In a closed aquifer, this storage amount is simply equal to the amount injected by the wells. In an open aquifer, this storage amount is equal to the amount injected minus the amount forecast to leak (if any). Then, the optimized storage efficiency is calculated using (1), where M_{co2} is equal to the optimized storage potential, and where CO_2 density and the aquifer's pore volume are known quantities.

Table A.3 summarizes the fluid and rock parameter inputs that we use in our flow simulations. In this work, we model residual trapping however neglect solubility trapping for three main reasons: to avoid using CO_2-brine solubility data from other modeling studies that is difficult to verify, to reduce the computational cost required to perform one forward simulation (we have to optimize the injection scenario for 23 individual formations, and each optimization problem requires numerous simulations), and to give a conservative estimate of storage potentials rather than an estimate that may include an optimistic amount of solubility trapping.

The optimization method explained above, as well as variants of (2), have been applied and documented in previous work; see e.g., [28, 29, 30, 21, 31], however for select formations. In Allen et al. [32], we obtained the dynamic storage efficiency of 23 of the formations available in NPD's CO_2 Storage Atlas [10], however all formations were treated as open systems. Herein, we apply this method to obtain closed system results for comparison purposes and to better represent the formations that are deemed to be closed.

2.3. Storage costs

Including the number of wells and well depths attempts to reflect some of the cost associated with exploiting the storage potential of the formation. Additionally, the cost of CO_2 transportation (via pipeline or ship) may be linearly related to the distance between the CO_2 point source and storage site. This is known as *source-sink* matching, and has been considered in other works, e.g., [33, 19].

To demonstrate our ranking workflow, we consider three possible Norwegian CO_2 point sources: a cement factory run by Norcem AS, an ammonia plant run by fertilizer maker Yara, and a trash incinerator run by the municipality of Oslo. These point sources are currently being considered as part of a feasibility study for a full-scale CCS demonstration project in Norway, where captured CO_2 would be transported by ship and injected into a Norwegian North Sea formation [34]. The location of these respective point sources and estimated annual emissions are:

1. Norcem in Brevik; location (539601, 6547015); $E_1 = 0.8$ Mt/yr [35]
2. Yara Porsgrunn in Herøya Industripark AS; location (535998, 6553803); $E_2 = 0.210$ Mt/yr [36]
3. Klemetsrudanlegget AS in Oslo; location (602917, 6635042); $E_3 = 0.3$ Mt/yr [37]

These emission rates suggest a total of 2 Mt/yr of CO_2 could become available for CO_2 storage, however we note that "full scale" capture might not necessarily mean 100% capture of CO_2 from the emission stream, as noted in Bjerge [35].

To represent transportation costs, we take the distance of an approximate shipping route between the CO_2 point source to the center of each formation; see Fig. 3. The center of each formation is determined by taking the mean (x, y) coordinate of the top surface.

Indeed, other storage related costs could be included, such as site development costs, monitoring costs, etc. (e.g., those used in Ramírez et al. [9]). However, the formations studied in this work are all categorized as offshore saline aquifers, thus these costs may not differ too much from case to case. As such, the number and depth of wells, and the distance from a point source are taken to be the only formation-dependent criteria related to storage costs.

2.4. Final ranking procedure

We propose a ranking scheme that prioritizes formations with the highest storage potential (s), highest injectivity (I), least number of wells (n), shallowest average well depth (z), highest degree of data coverage (u), and closest proximity to CO_2 point source j (d_j). Following the weighted normalized parametric procedure presented in [1, 19], the ranking of formation k with respect to point source j, is computed by

$$R_j^k = \sum_{i=1}^{6} w_i C_i^k, \tag{4}$$

where C is the normalized parameter for each of the criteria, which are indexed using the subscript i, i.e.,

$$\begin{aligned} C_1^k &= \frac{s^k - s_{\min}}{s_{\max} - s_{\min}}, \quad C_2^k = \frac{I^k - I_{\min}}{I_{\max} - I_{\min}}, \quad C_3^k = \frac{u^k - u_{\min}}{u_{\max} - u_{\min}}, \quad C_4^k = \frac{n_{\max} - n^k}{n_{\max} - n_{\min}}, \\ C_5^k &= \frac{z_{\max} - z^k}{z_{\max} - z_{\min}}, \quad C_6^k = \frac{d_{j,\max} - d_j^k}{d_{j,\max} - d_{j,\min}}. \end{aligned} \tag{5}$$

The max and min subscripts indicate the maximum and minimum value out of all the formations being ranked. The non-normalized storage potential, s, is the optimized value depending on whether the formation is considered to be open or closed. Even though we are already using s which is simulation-based and thus indirectly includes

Figure 3: Approximate shipping route that may be taken from a CO_2 point source in Porsgrunn to the center of the Garn formation. Figure constructed using Google Maps [38]. Yellow stars in Norwegian North Sea indicate the center of other formations. Outline of Garn formation is approximate.

all the main properties to calculate well injectivity, we include $k(x)h(x)$ in our ranking scheme as a weak indicator of injectivity I. This criterion is used to reflect the most important variations in local well performance. The weighting coefficients w_i express the relative importance of each parameter to the overall ranking, and sum up to unity, i.e., $\sum_i^6 w_i = 1$. To account for uncertainty associated with the formation datasets, we use a numeric value between 1 and 3 that represents the quality of the data coverage. We interpret these values based on the color that is used in the NPD Atlas [10] (i.e., red, yellow, or green) to indicate the maturity of each formation's storage estimate.

3. Results

3.1. Optimized storage potentials, efficiency, & categorization

The optimized storage potentials and efficiency factors are computed according to the methodology explained in Sect. 2.2. Whether or not fluid is able to transmit in and out of the formation's lateral boundaries will impact the storage potential of the aquifer. For comparison purposes, we obtain the optimal storage potentials for both possible boundary conditions; see Fig. 4. The same well locations were used in both system types since it is still ideal to place wells downslope from local structural traps and at low elevations within a catchment region. Placing wells at low elevations is particularly important to benefit from residual trapping that occurs as CO_2 migrates towards the higher elevations, to reduce the risk of CO_2 leakage through wells, and also because the pressure is less restrictive at deeper elevations since the overburden pressure is higher.

From Fig. 4, we notice that the open storage efficiencies fall within the range of 0.3 – 4.2% (excluding Pliocenesand because its structural trapping capacity is practically negligible), and all the closed storage efficiencies are less than 1%. We also notice that most of the closed storage efficiencies are less than the open storage efficiencies. The reason for this is primarily due to the lack of pressure dissipation and resulting over-pressure in closed boundary systems. Pressure management techniques such as brine extraction is one way to release the pressure buildup caused by CO_2 injection.

However, there are a few formations, e.g., Hugin East, Hugin West, and Pliocenesand, that do not exhibit lower storage efficiencies for closed boundaries. The reason for this is related to the shape of the top-surface and the limited amount of structural trapping potential; see Fig. 5. When these formations are closed, lateral boundary leakage does not exist, and thus does not restrict the injection mass. The only limitation is due to pressure. In fact, the top surface of these closed formations are in essence one large structural trap. So, as

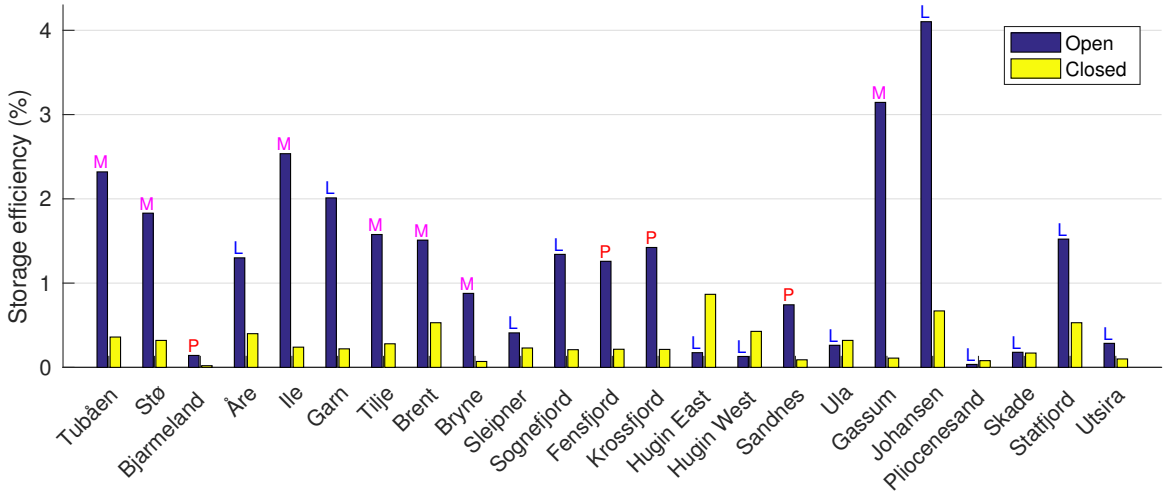

Figure 4: Comparison between open and closed storage efficiencies obtained through optimization of injection rates. Symbols above open results refer to whether optimal injection strategy was limited due to leakage ("L"), pressure ("P"), or a mixture of both ("M").

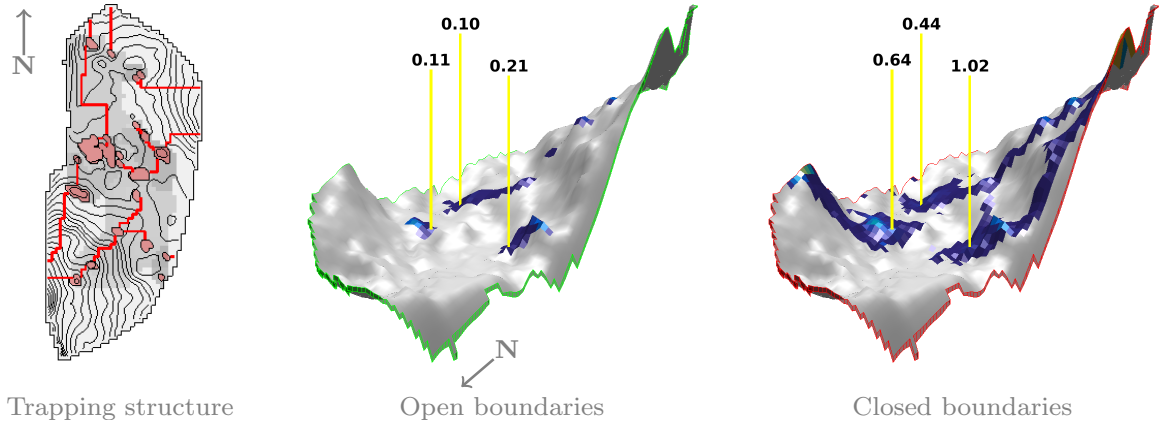

Figure 5: Optimized injection rates (in Mt/year) given a 30-year injection period in Hugin East when the formation is treated as open or closed.

long as the wells are operating such that the pressure rise within these formations is within the predefined tolerance of the pressure target, more CO_2 can be injected than what the (open) structural trapping potentials suggest. On the other hand, the injection rates are lower when these systems are assumed to be open because any additional CO_2 injected into the formations will spill out of their already limited structural traps. It may be possible to obtain an even higher S_{eff} value through the use of a different well placement, e.g., an array of wells that spans the entire areal coverage of the top-surface. This hypothesis will be tested and discussed later in Fig. 9.

When formations are treated as open systems, the optimal strategy may be limited either by excess CO_2 leakage from the lateral boundaries, or by excess pressure buildup. As such, we categorize injection strategies of the open formations in terms of what limited the injection of more CO_2. Fig. 6 illustrates each possible type of limitation. In closed systems, no CO_2 leakage occurs from the lateral boundaries, and thus pressure will be the limiting factor in all cases. The relevance for this type of categorization is related to engineering strategies that one could take to increase the storage capacity of the formation. For example, to inject more CO_2 into a leakage-limited formation, it may be necessary to consider strategies which reduce the mobility of CO_2, such as CO_2 and water alternating injection, etc. To inject more CO_2 into a pressure-limited formation, it may be necessary to include brine producing wells for pressure management or increase the injection period. This last strategy comes from the fact that an aquifer's storage capacity (as well its categorization or storage constraint) is dependent on the duration of the injection period, which has been discussed in Szulczewski et al. [39] and Bachu [18]. In one of our previous studies, i.e., [32], we illustrated this point by comparing optimized storage capacities given two different injection time frames. In almost all cases, the storage efficiency of an open system increased when the injection period was increased from 30 to 100 years. And in several of these

cases, the storage constraint switched from pressure-limited (or a combination of pressure and leakage-limited) to leakage-limited.

According to the results shown in Fig. 4, most of the formations are limited by leakage only, or a combination of leakage and pressure. A few formations—Bjarmeland and Sandnes—were limited purely by pressure buildup. In cases where pressure was a limiting factor, the pressure reached its predefined pressure target at locations surrounding an injection well (e.g., Tilje in Fig. 6) or within a shallow trap (e.g., Bjarmeland in Fig. 6). This indicates that while it is considered advantageous to place wells within the deepest regions of a formation where the overburden pressure is highest (thus the pressure limit is least restrictive), the amount to safely inject into the formation may ultimately be dictated by the maximum sustainable pressure rise that occurs in the shallowest traps where the overburden pressure is smallest.

3.2. Overall ranking

The six criterion values for each formation are given in Table 2, along with four possible combinations of criterion weighting. Using these cases, the ranking (R) of each formation was computed using (4), and results are presented in Fig. 7. The storage potentials that we report under criterion s correspond to either the open or closed optimals. The information we used to say whether a formation is open or closed was taken from the NPD Atlas, with the following assumptions: in cases where the formation was said to be half-open, we treated it as open, and in cases where the system type was not specified, we treated it as closed. Also, we only consider the Porsgrunn point source, since all three CO_2 point sources we referenced in this work are concentrated in southern Norway and thus lead to very similar ranking results.

Since the overall ranking is dependent on which criteria are used, and the relative importance of each criterion, we tested out a few possible weighting combinations. In Case A, we treat the storage potential as the most important ranking criterion ($w_s = 0.5$), following by the combined impact of the three economic criteria (i.e., each assigned a weight of 0.1, thus combined impact of 0.3), and the least important was data coverage ($w_u = 0.15$) and injectivity ($w_I = 0.05$). In Case B, all criteria are given equal importance in the overall ranking. In Case C and D, we set the relative importance of the distance to the CO_2 point source to $w_d = 0.3$, however we compare the impact of using only the *simulation*-based criteria (i.e., optimized storage potential, number of wells placed by our algorithm, and depth of wells) to using only the *static*-based criteria (i.e., injectivity and quality of data coverage). Results of these ranking cases are presented in Fig. 7.

The ranking values shown for Case B in Fig. 7 includes upper and lower bounds (shown by blue "error bars"), which indicate the range of possible ranking values for each formation. As an example, the normalized criteria for Utsira are $\mathbf{C} = \{0.2787, 0.8911, 0.5833, 0.8779, 1.0000, 0.8328\}$ (i.e., the criterion values in Table 2 normalized by (5)). From this array of values, we notice that the highest possible ranking value for Utsira will be 1.0 (which occurs when $w_5 = 1$, i.e., ranking is based on the degree of data coverage criterion only), and the lowest possible value will be 0.2787 (when $w_1 = 1$, i.e., ranking is based on the optimized storage criterion only). So, no matter what combination of weighting coefficients we use, the ranking value for Utsira will always fall within the bound of $[0.2787, 1.0]$. Computing the ranking bounds could help identify any formations that should be eliminated from the list of candidate storage sites, especially if a formation has a very low upper bound compared to all other formations. Based on the ranking bounds plotted in Fig. 7, we observe that Åre has the worst upper bound value, and Utsira has the best lower bound. However, these particular ranking bounds do not strongly suggest a particular formation to eliminate.

According to Anthonsen et al. [13], Utsira, Sognefjord, and Skade were considered to be the best formations for large-scale industrial storage. Thus in Fig. 7, we highlight the score of these formations to compare how their position in the ranking order changes between the different weighting cases. Utsira and Skade score as the two best formations when ranking is based on the static data only (Case D), presumably because their high injectivity values. They also score as the top best when all criteria are given equal importance (Case B), with Sognefjord coming in third. However, when the optimal storage potentials are weighted as most important in Case A and C, Utsira, Skade and Sogenfjord drop from their high scoring positions. This is likely due other formations having higher storage potentials, such as Statfjord, which ranks the number one in terms of optimized capacity. For comparison, we illustrate the optimized rates and final CO_2 saturations in Anthonsen et al.'s [13]'s "best three" formations and in Statfjord; see Fig. 8. Our optimized storage potentials indicate it may be possible to trap more CO_2 in the Statfjord formation, compared to Utsira, Skade, or Sognefjord.

Our intention here is not to make any definitive remarks about which formations are the most suitable for large-scale industrial storage, due to the simplifications and working assumptions discussed in the next section. Rather, our purpose is to demonstrate that a formation's ranking score may very well change should optimal storage potentials and economic factors be incorporated into the ranking scheme.

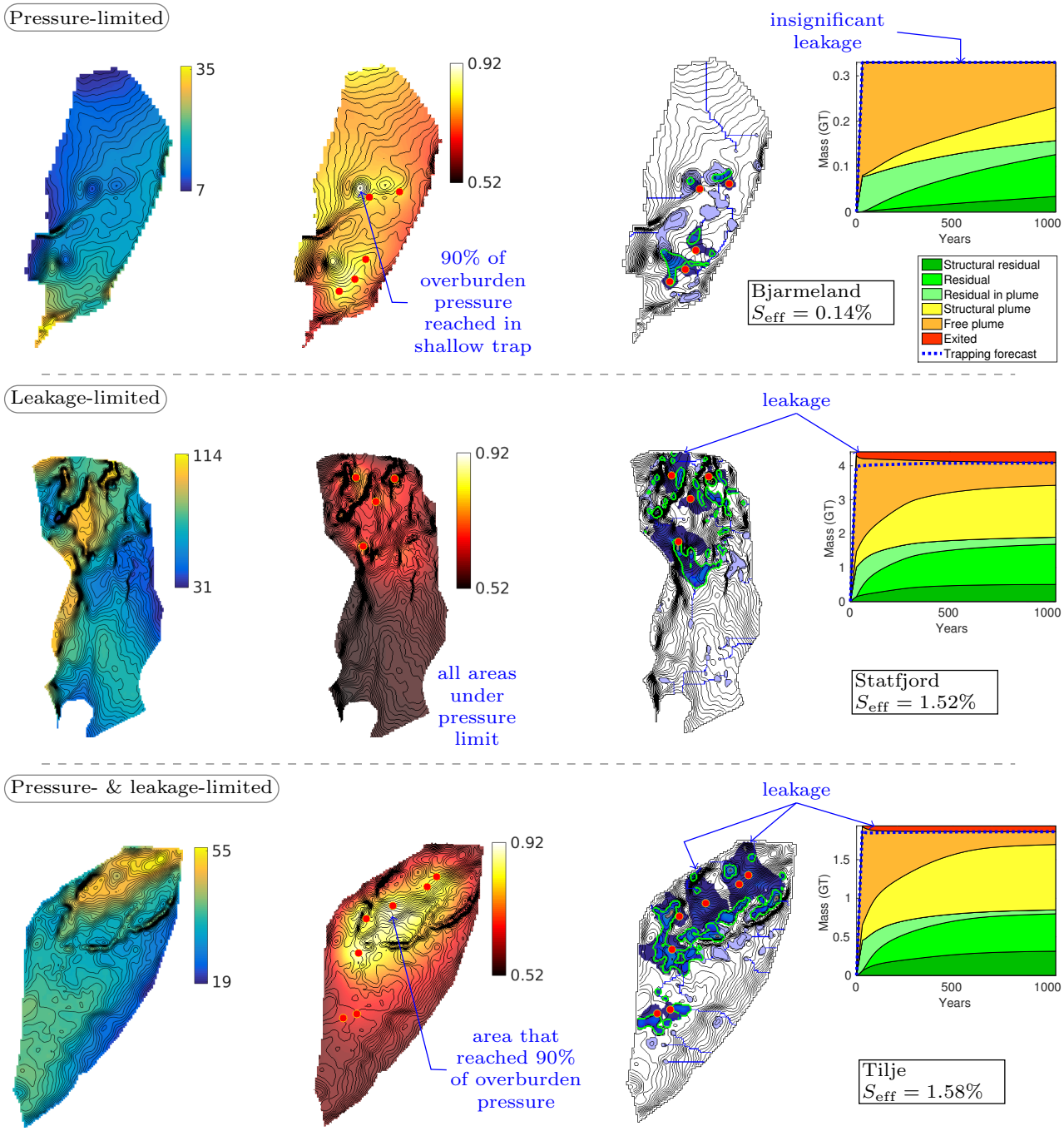

Figure 6: Examples of three different categories of open-system injection strategies, in terms of what limited the storage efficiency. *Left to right*: overburden pressure (in MPa), fraction of overburden pressure reached, CO_2 saturation after 1000 years, and trapping inventory. Optimized examples were obtained using a 30-year injection period and a leakage penalty factor of 5. Fraction of overburden pressure reached is with respect to the entire simulation period, and indicates the locations where pressure reached or approached its pressure target within a factor of safety. S_{eff} is storage efficiency.

Table 2: Values of criteria used in formation ranking. Non-normalized values given. Meaning of symbols: s – optimized storage potential (Mt), I – injectivity ($\times 10^{-12}$ m^3), n – number of wells to operate, z – average depth of wells (m), u – degree of data coverage, d_j – distance (km) to point source j. Storage and well details are with respect to open or closed systems. Systems treated as closed (*): Hugin West, Brent, Ula, Pliocenesand, Tilje, Åre, Garn, Ile. Rest of systems considered to be open.

	Criterion i					
Formation k	s	I	n	z	u	d_1
Tubåen	555	8.6	4	2683	3.00	2044
Stø	667	13.9	5	2264	3.00	2044
Bjarmeland	330	12.2	5	1224	2.50	2258
Åre	* 768	35.9	8	2927	2.00	1190
Ile	* 110	29.7	7	2277	2.00	1190
Garn	* 233	82.6	4	1997	2.00	1190
Tilje	* 332	20.8	7	2578	2.00	1190
Brent	* 2700	81.2	8	4111	1.00	654
Bryne	3032	14.2	14	2303	2.00	377
Sleipner	98	26.2	2	3676	1.00	539
Sognefjord	1503	28.6	3	1903	3.00	615
Fensfjord	1500	30.8	4	1857	3.00	615
Krossfjord	1384	24.2	3	1893	3.00	615
Hugin East	13	20.2	3	2864	3.00	556
Hugin West	* 126	33.7	3	3237	1.00	539
Sandnes	613	5.1	13	2226	2.00	386
Ula	* 147	26.0	4	3952	1.00	491
Gassum	1197	32.0	2	2320	1.00	238
Johansen	1686	31.8	4	2436	3.00	599
Pliocenesand	* 5	42.2	5	535	1.00	606
Skade	410	177.0	9	1011	3.00	568
Statfjord	4083	26.9	4	4918	2.00	620
Utsira	1141	158.3	7	1070	3.00	576
Weighting Case						
A	0.50	0.05	0.10	0.10	0.15	0.10
B	0.1670	0.1666	0.1666	0.1666	0.1666	0.1666
C	0.50	-	0.10	0.10	-	0.30
D	-	0.35	-	-	0.35	0.30

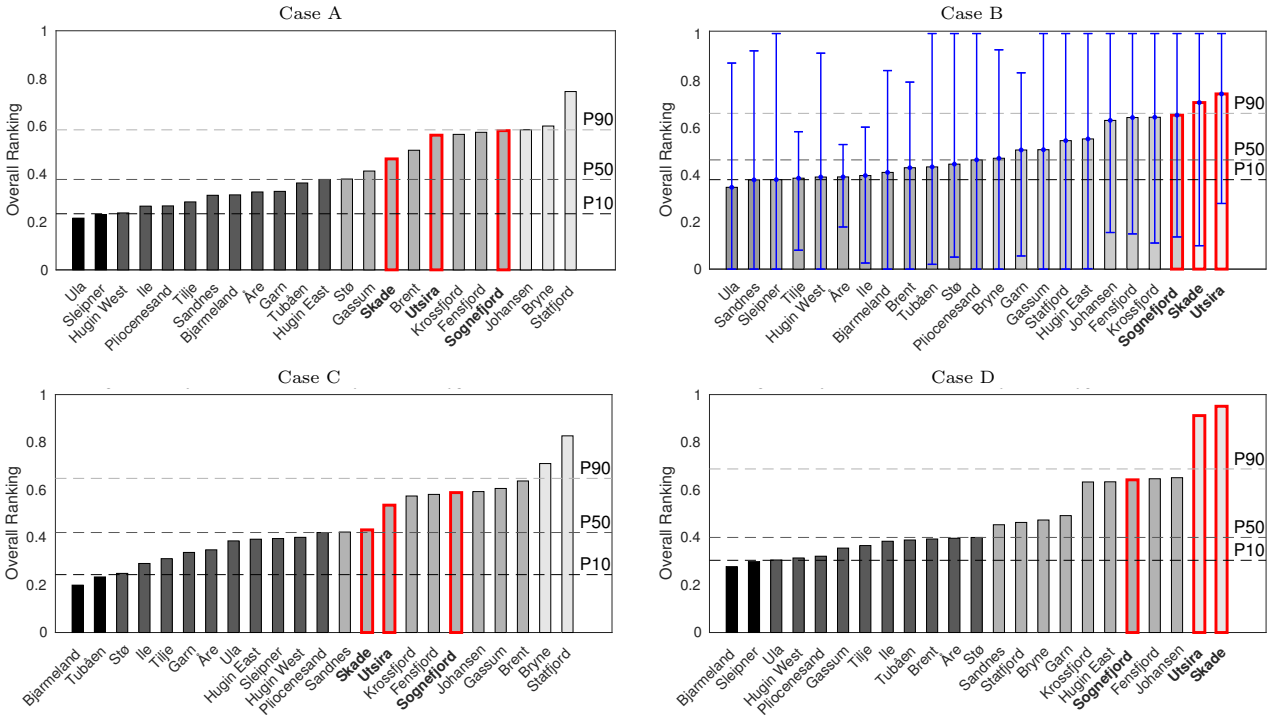

Figure 7: Formation ranking according to several different weight combinations. Ranking scores of Utsira, Skade, and Sognefjord formations are outlined in red for easier visualization of how their position changes between the weighting cases. These results are not intended to be used as definitive ranking scores.

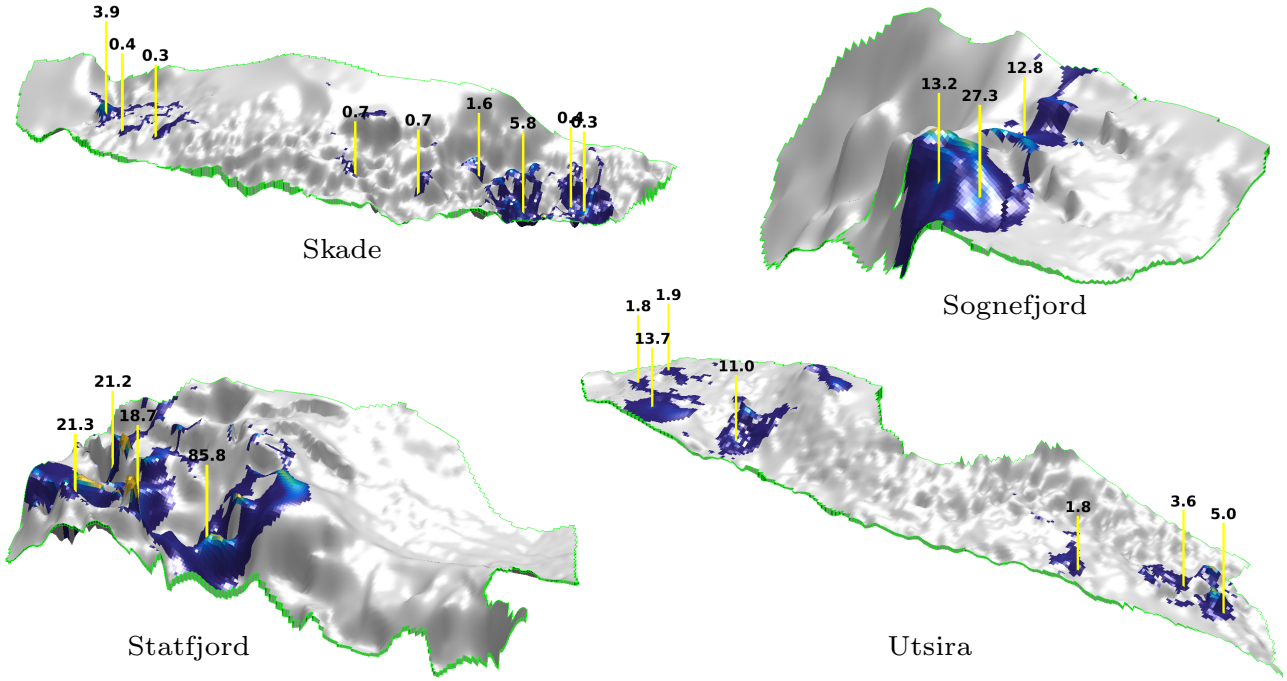

Figure 8: Optimized injection rates (in Mt/yr), given a 30-year injection period, in select formations. CO_2 saturation after 1000 years of post-injection migration is shown. Yellow lines represent an injection "hub" consisting of multiple injectors, not necessarily just one well.

4. Discussion

4.1. Influence of working assumptions

The results of our ranking procedure are influenced by several factors and working assumptions. Firstly, our optimized storage potentials represent only one realization of homogeneous formation properties, a particular well placement strategy, and a particular injection strategy which included an injection period of 30-years. To better account for dataset uncertainty, optimized storage potentials could be obtained using many realizations of top-surface elevations, rock properties, or other potentially impactful and uncertain parameters. While the same well placement algorithm (i.e., modified greedy) was used for both open and closed formations, it is possible that storage potentials could be higher if the open formation's top-surface was covered with an array of injection wells. This is confirmed in Fig. 9, where we compare the optimized storage efficiencies for three different well placement strategies, on a coarsely resolved Sandnes grid, using a 30-year injection and a relatively short migration period of 200 years. On the other hand, using more wells may end up reducing the final ranking of the formation due to economic factors (i.e., more wells means higher cost). In a previous work, we demonstrated that the optimal injection strategy depends on the length of the injection period [32]. As such, we expect that using an injection period of 10- or 50-years would yield different results than for 30-years.

Secondly, the working assumptions we used in our optimization approach included a leakage penalty factor of five and a pressure target of 90% of the overburden pressure. If political regulations required essentially no CO_2 leakage from the formation and allowed for a very small over-pressure, then a higher leakage penalty factor and a stricter pressure target should be applied when optimizing the injection rates. This would most certainly yield different (i.e., lower) storage potentials.

Thirdly, we only considered certain criteria in our ranking procedure. The same procedure could be applied using a different set of criteria, or using volumetric or structural trapping potentials instead of the optimized storage amounts. Once again, one would expect to find different ranking values, given the difference between the volumetric storage estimates in Table 1 and the optimized storage potentials in Table 2. However, an important aspect of using optimized storage potentials is that details of the injection scenario (e.g., number of wells, well location) and legal or political requirements (e.g., amount of long-term leakage allowed, maximum allowable pressure buildup) can be accounted for in the estimate.

Fourthly, weighting coefficients were used according to an assumption of how important each criterion was in the overall evaluation. The comparison we made in Fig. 7 demonstrates that the score of a formation can very well change depending on which criteria are included, and their relative importance.

Our interpretation of the formation datasets has also influenced the ranking results. We have considered each formation separately, however it is known that some of these formations form aquifer units, such as the

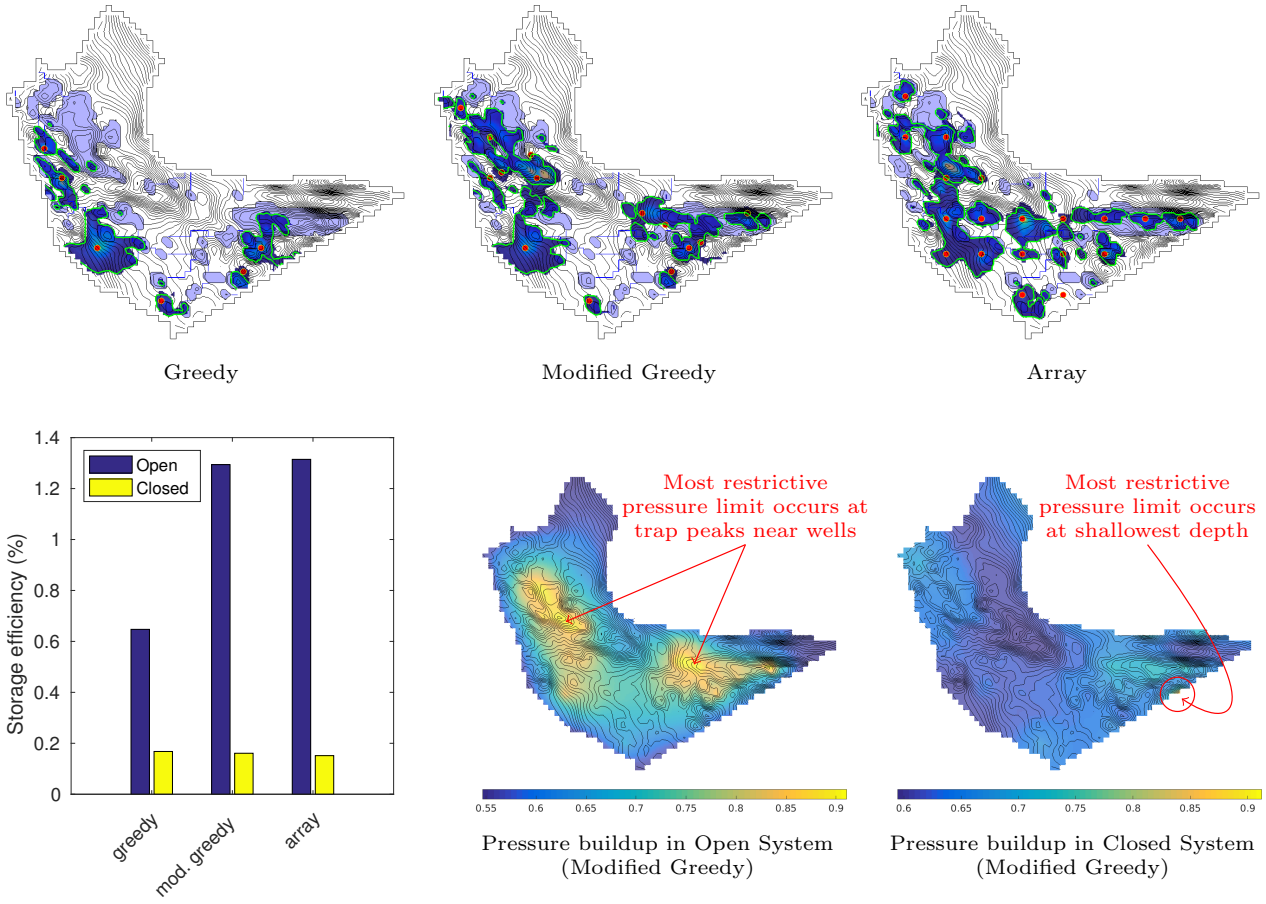

Figure 9: Impact of well placement on optimal storage potential. *Top row*: placement of wells in Sandnes formation using three different strategies, and CO_2 saturation by year 230 when wells operated with their optimized rates (for an open system). *Bottom left*: optimized storage efficiencies given three well placement approaches, and given an open or closed system. *Bottom right*: maximum pressure reached (expressed as a fraction of the overburden pressure) when system treated as open or closed, using the modified greedy well placement.

Sognefjord Delta (Sognefjord, Fensfjord, and Krossfjord), and the Hammerfest Aquifer Basin (Stø and Tubåen). It is likely that treating the units as a whole instead of separately would have led to different values of optimized storage potentials, and thus different ranking. When information was missing (e.g., boundary conditions), we made assumptions regarding the characteristics of the formation.

By considering a CO_2 point source located in southern Norway, the outcome of the ranking procedure is more favorable for the Norwegian North Sea formations. If we had considered a hypothetical CO_2 point source located in northern Norway, we expect to find that the ranking scores of the Barents Sea formations would be higher than shown in this study. Also, site selection could very well depend on a source's CO_2 emission rate E_j due to financial reasons associated with project length. For example, a project will need to operate for 50 years in order to store 1 Gt of CO_2 coming from a point source with an emission rate of $E_j = 2$ Gt/year, however it will take less time (20 years) to store the same amount if the emission rate is $E_j = 5$ Gt/year. This dependency could have been accounted for by expressing the storage potentials as s/E_j, as done in Bachu et al. [3] for CO_2-EOR projects. However, in this work, the optimized storage potentials correspond to a fixed injection period of 30 years and assumed unlimited CO_2 availability. We note that the assumed emission rates of the three CO_2 point sources provides a total of approximately 40 Mt over a 30-year period. Yet most of our optimized storage potentials suggest that much more CO_2 would have to be available if one wanted to exploit the full storage potential of a formation within a reasonable time frame.

4.2. Comparison to other ranking procedures

The formations found along the Norwegian Continental Shelf have been subject to previous ranking procedures. In Anthonsen et al. [13], 27 Norwegian sites (in addition to Swedish, Danish and Icelandic sites) were mapped and characterized with respect to reservoir and seal properties, safety, and data coverage. Based on the ranking methodology applied, ten of these sites were considered as most prospective storage formations,

namely: Sognefjord, Krossfjord, Utsira, Skade, Heimdal, Fensfjord, Frigg, Garn, Johansen, and Statfjord. And out of these, Utsira, Sognefjord, and Skade were said to be the best formations for large-scale CO_2 storage, given their large volumetric storage capacities, shallow depths, and high porosity and permeability values.

Our study considered eight of the "top ten" formations listed above (i.e., Heimdal and Frigg are not part of NPD's public dataset). It is interesting to note that seven of these eight formations ranked in the top 50th percentile of the overall ranking shown in Fig. 7, even though our ranking methodology was different. (Garn did not rank as favorably, because it is located in the Norwegian Sea, which is much farther from the assumed CO_2 point source than the North Sea formations.) We considered criteria related to storage costs and optimized storage potentials, while Anthonsen et al. [13] did not factor in any costs and only factored in volumetric storage potentials when two or more sites had the same ranking score.

Including qualitative criteria such as data coverage is useful because it helps to represent the uncertainty associated with data, which likely influenced the storage capacity estimates. In an effort to further rank Anthonsen et al.'s [13] top ten Nordic sites with more qualitative measures, Bergmo et al. [14] included a "knowledge gap" score (complementary to a "readiness level" score). This "readiness level" score was determined by assigning a numeric value between 0 and -3 to knowledge gaps related to data collection, modelling, characterization of sensitivity, and risk assessment. The rationale behind this is formations that have been subject to a lot of data collection, characterization, and assessment are considered to be more ready to serve as CO_2 storage sites. While we only included quality of data coverage into our ranking procedure, this "readiness level" could serve as an additional criterion.

5. Conclusions

In this work, we have presented a ranking procedure and applied it to 23 saline aquifer formations located along the Norwegian Continental Shelf, to determine which formations may be deemed as most suitable for CO_2 storage. This ranking approach was based on the weighted normalized parametric procedure used in Bachu [1] and Bachu [19]. The parameters used to evaluate the overall ranking included optimized storage potentials, injectivity, number of wells, depth of wells, degree of data coverage, and distance from a CO_2 point source.

A key feature of our ranking procedure is simulation based quantities based on automatic algorithms and optimization. Optimized storage potentials were obtained by first placing wells with a generic scheme, and then by performing mathematical optimization of injection rates using vertical-equilibrium simulation and a set of working assumptions related to maximum allowable leakage and pressure buildup. Simulation based quantities capture more of the operational, legal, and economical constraints involved in a CCUS project, compared to simple volumetric based estimates. With simulations, sweep efficiency is more accurately accounted for, and it is easier to evaluate competing dynamic features which are dependent on injection time frame (e.g., injecting a fixed amount over a short versus long time frame produces different leakage pathways and residual trapping amounts). While we have employed vertical-equilibrium (VE) modeling in our work for computational efficiency, this ranking workflow is not limited to VE and 3D flow simulations could also be used. Another important feature of our ranking workflow is that criteria such as number and depth of wells, and distance to a CO_2 point source attempts to capture the storage costs involved, particularly regarding CO_2 transport and injection.

The results of our demonstrated ranking procedure are not intended for engineering purposes due to a variety of simplifications (e.g., homogeneous rock properties, neglecting faults, grid coarsening) included in the geomodels. However, our demonstrated workflow can be applied to more detailed datasets and used as a screening tool to aid in the selection of formations considered to be the most suitable storage candidates. Once the "best" sites are identified, more detailed investigations could be performed to further narrow down these candidates. The final selection will likely need to account for what is realistically feasible in a CO_2 storage project, particularly related to engineering and financial aspects.

Acknowledgements

This work was funded in part by the Research Council of Norway through grant no. 243729 (Simulation and optimization of large-scale, aquifer-wide CO_2 injection in the North Sea).

Appendix A.

Table A.3: Properties of formation rock and fluid found along the Norwegian Continental Shelf. Where no reference is given, values have been either computed or assumed based on other sea data (e.g., Barents seabed temperature computed to meet Tubåen conditions reported in Pham et al. [40]). Compressibility values correspond to a reference pressure of 10 MPa.

	Sea values and references						
Parameter	Barents	Ref.	Norwegian	Ref.	Norwegian North	Ref.	Unit
Sea depth	330	[10]	225	-	100	-	m
Seabed temp.	4	-	5	[41]	7	[42]	°C
Thermal gradient	40	[10]	41.3	[41]	35.6	[42]	°C/km
Residual water sat.	0.11	-	0.11	-	0.11	[42]	unitless
Residual CO_2 sat.	0.21	-	0.21	-	0.21	[42]	unitless
Water density	1100	[10]	1020	-	1020	[42]	kg/m^3
Water viscosity	8×10^{-4}	-	8×10^{-4}	-	8×10^{-4}	[42]	$Pa \cdot s$
CO_2 viscosity	6×10^{-5}	-	6×10^{-5}	-	6×10^{-5}	[42]	$Pa \cdot s$
Water compressibility	4.3×10^{-5}		4.3×10^{-5}		4.3×10^{-5}		bar^{-1}
Rock compressibility	1.0×10^{-5}		1.0×10^{-5}		1.0×10^{-5}		bar^{-1}

Table A.4: Grid coarsening details and buffer distances used to place wells. Buffer letter meaning: A – to internal catchment boundary, B – to formation boundary, C – to external catchment boundary, D – to other wells placed in same catchment, E – n wells placed in same catchment, in best k catchments, i.e., $(n_1, n_2, \ldots, n_k)$.

	Coarsened grid details			Buffers				
Formation	Coarsening	Cell Size (m)	# cells	A (km)	B (km)	C (km)	D (km)	E
Tubåen	2	1000	6426	3	10	10	-	(1,1,1)
Stø	2	1000	6426	5	15	5	20	(3)
Bjarmeland	4	2000	7832	2	30	20	20	(2,1,1)
Åre	8	1600	7643	2	15	10	30	(2)
Ile	8	1600	8388	2	15	10	40	(2)
Garn	8	1600	6943	3	20	17	20	(2)
Tilje	8	1600	8019	3	18	14	20	(1)
Brent	2	2000	5019	5	20	15	20	(2,2)
Bryne	2	2000	11197	5	15	15	20	(4,4)
Sleipner	1	1000	5290	2	5	2	-	-
Sognefjord	1	1000	9383	5	10	8	15	(2)
Fensfjord	1	1000	9263	5	10	8	15	(3)
Krossfjord	1	1000	9640	5	10	8	15	(2)
Hugin East	1	1000	2264	2	5	2	-	-
Hugin West	1	1000	5540	2	5	2	-	-
Sandnes	2	2000	10840	5	15	15	20	(6,3)
Ula	1	1000	4544	2	8	2	-	-
Gassum	3	1500	3405	5	10	8	-	-
Johansen	3	600	8476	2	5	5	15	(2,1)
Pliocenesand	1	500	13859	1	3	1	-	-
Skade	2	1000	12736	2	10	5	-	-
Statfjord	3	1500	13160	5	20	5	-	-
Utsira	3	1500	10220	3	10	10	-	-

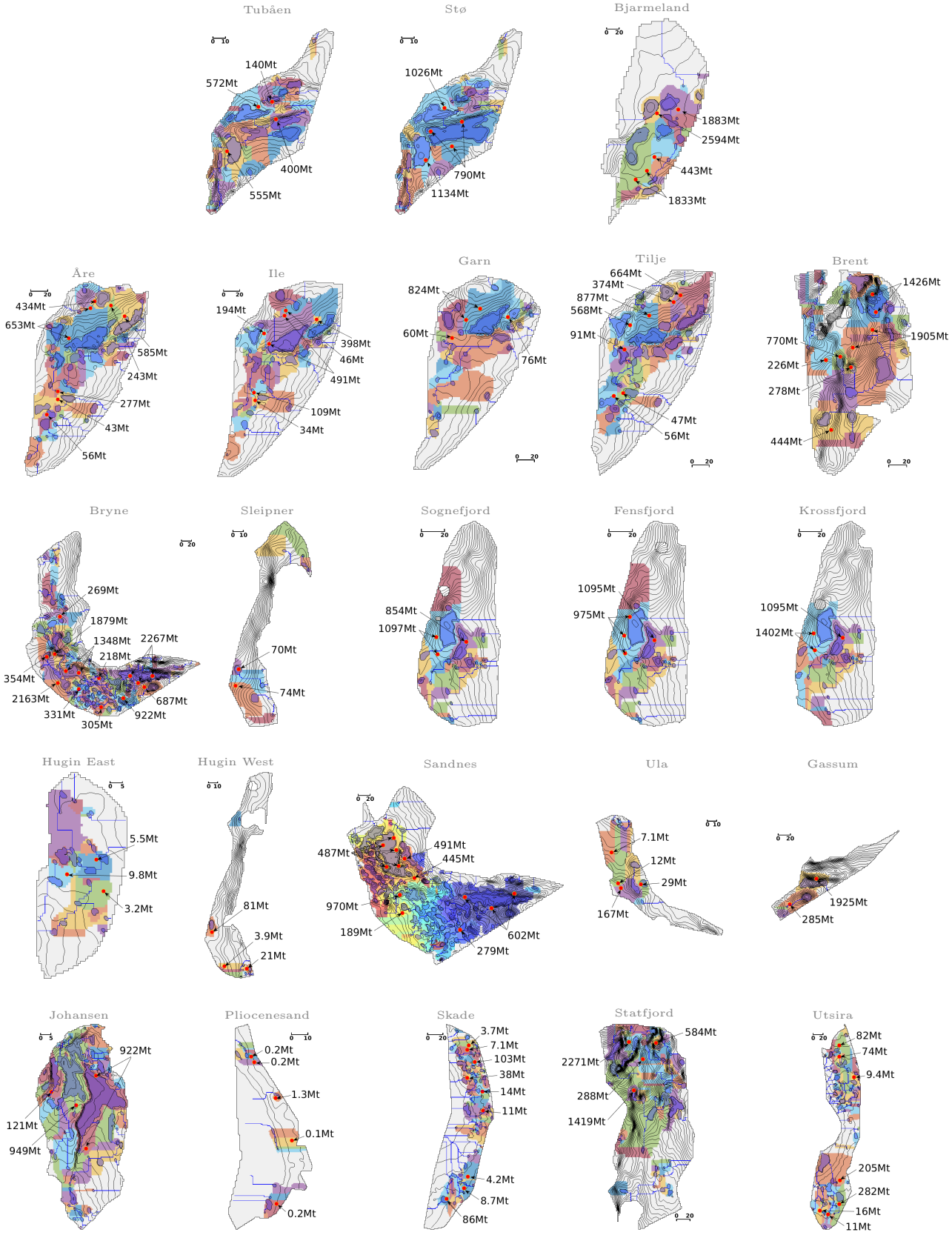

Figure A.10: Well placement and initial injection masses. Scale is indicated (in km) for each formation. Contour lines are drawn at 150 meter intervals. Wells are indicated by red dots. Color palate used for trapping structure: catchment regions are distinguished using random colors, structural traps are shown using a darker shade of its catchment region's color, and connections between traps (i.e., spill-paths) are indicated by blue lines.

[1] S. Bachu, Screening and ranking of sedimentary basins for sequestration of CO2 in geological media in response to climate change, Environmental Geology 44 (3) (2003) 277–289. doi:10.1007/s00254-003-0762-9.

[2] U.S. Department of Energy, Office of Fossil Energy, Carbon Storage Atlas, 5th Edition, netl.doe.gov/research/coal/carbon-storage/atlasv (2015).

[3] S. Bachu, A. Melnik, R. Bistran, Approach to evaluating the CO2 storage capacity in Devonian deep saline aquifers for emissions from oil sands operations in the Athabasca area, Canada, Energy Procedia 63 (2014) 5093–5102. doi:10.1016/j.egypro.2014.11.539.

[4] B. E. Bradshaw, L. K. Spencer, A.-L. Lahtinen, K. Khider, D. J. Ryan, J. B. Colwell, A. Chirinos, J. Bradshaw, J. J. Draper, J. Hodgkinson, M. McKillop, An assessment of Queensland's CO2 geological storage prospectivity–The Queensland CO2 geological storage atlas, Energy Procedia 4 (2011) 4583–4590. doi:10.1016/j.egypro.2011.02.417.

[5] M. Cloete, Atlas on geological storage of carbon dioxide in South Africa, Tech. rep., Council for Geoscience, Johannesburg, South Africa, sacccs.org.za/wp-content/uploads/2010/11/Atlas.pdf (2010).

[6] D. Lewis, M. Bentham, T. Cleary, R. Vernon, N. O'Neill, K. Kirk, A. Chadwick, D. Hilditch, K. Michael, G. Allinson, P. Neal, M. Ho, Assessment of the potential for geological storage of carbon dioxide for the island of Ireland, Tech. rep., Sustainable Energy Ireland, Environmental Protection Agency, Geological Survey of Northern Ireland, and Geological Survey of Ireland, seai.ie/News-Events/Press-Releases/Storage-of-CO2-Report-Sept-08.pdf (2008).

[7] F. E. Watson, S. A. Mathias, S. E. Daniels, R. R. Jones, R. J. Davies, B. J. Hedley, J. van Hunen, Dynamic modeling of a UK North Sea saline formation for CO2 sequestration, Petrol. Geosci. 20 (2) (2014) 169–185. doi:10.1144/petgeo2012-072.

[8] M. Bentham, T. Mallows, J. Lowndes, A. Green, CO2 STORage Evaluation Database (CO2 Stored): The UK's online storage atlas, Energy Procedia 63 (2014) 5103–5113. doi:10.1016/j.egypro.2014.11.540.

[9] A. Ramírez, S. Hagedoorn, L. Kramers, T. Wildenborg, C. Hendriks, Screening CO2 storage options in The Netherlands, International Journal of Greenhouse Gas Control 4 (2) (2010) 367–380. doi:10.1016/j.ijggc.2009.10.015.

[10] E. K. Halland, J. Mujezinović, F. Riis (Eds.), CO_2 Storage Atlas: Norwegian Continental Shelf, Norwegian Petroleum Directorate, 2014, npd.no/en/Publications/Reports/Compiled-CO2-atlas.

[11] R. Bøe, C. Magnus, P. T. Osmundsen, B. I. Rindstad, CO2 point sources and subsurface storage capacities for CO2 in aquifers in Norway, Tech. rep., Geological Survey of Norway, Trondheim, ngu.no/FileArchive/101/2002 010 skjerm.pdf (2002).

[12] Geological Survey of Denmark and Greenland, Nordic CO2 storage atlas, data.geus.dk/nordiccs/.

[13] K. Anthonsen, P. Aagaard, P. Bergmo, S. Gislason, A. Lothe, G. Mortensen, S. Snæbjörnsdóttir, Characterisation and Selection of the Most Prospective CO2 Storage Sites in the Nordic Region, Energy Procedia 63 (2014) 4884–4896. doi:10.1016/j.egypro.2014.11.519.

[14] P. E. S. Bergmo, B. U. Emmel, K. L. Anthonsen, P. Aagaard, G. M. Mortensen, A. Sundal, Quality ranking of the best CO2 storage aquifers in the Nordic countries, in: GHGT-13 – 13th International Conference on Greenhouse Gas Control, Lausanne, Switzerland, 14 – 18 November 2016, Energy Procedia, 2017.

[15] A. Goodman, A. Hakala, G. Bromhal, D. Deel, T. Rodosta, S. Frailey, M. Small, D. Allen, V. Romanov, J. Fazio, N. Huerta, D. McIntyre, B. Kutchko, G. Guthrie, U.S. DOE methodology for the development of geologic storage potential for carbon dioxide at the national and regional scale, International Journal of Greenhouse Gas Control 5 (4) (2011) 952–965. doi:10.1016/j.ijggc.2011.03.010.

[16] T. Grant, D. Morgan, A. Poe, J. Valenstein, FE/NETL CO2 Saline Storage Cost Model: User's Manual, Tech. Rep. DOE/NETL-2012/1582, National Energy Technology Laboratory (2014).

[17] D. Morgan, T. Grant, FE/NETL CO2 Saline Storage Cost Model: Model Description and Baseline Results, Tech. Rep. DOE/NETL-2014/1659, National Energy Technology Laboratory (2014).

[18] S. Bachu, Review of CO2 storage efficiency in deep saline aquifers, Int. J. Greenh. Gas Con. 40 (2015) 1–15. doi:10.1016/j.ijggc.2015.01.007.

[19] S. Bachu, Identification of oil reservoirs suitable for CO2-EOR and CO2 storage (CCUS) using reserves databases, with application to Alberta, Canada, International Journal of Greenhouse Gas Control 44 (2016) 152–165. doi:10.1016/j.ijggc.2015.11.013.

[20] H. M. Nilsen, K.-A. Lie, O. Møyner, O. Andersen, Spill-point analysis and structural trapping capacity in saline aquifers using MRST-co2lab, Computers & Geosciences 75 (2015) 33–43. doi:10.1016/j.cageo.2014.11.002.

[21] K.-A. Lie, H. M. Nilsen, O. Andersen, O. Møyner, A simulation workflow for large-scale CO2 storage in the Norwegian North Sea, Comput. Geosci. 20 (3) (2016) 607–622. doi:10.1007/s10596-015-9487-6.

[22] J. M. Nordbotten, M. A. Celia, Geological Storage of CO2: Modeling Approaches for Large-Scale Simulation, John Wiley & Sons, Inc., 2012.

[23] P. Wolfe, Convergence conditions for ascent methods, SIAM Rev. 11 (2) (1969) 226–235. doi:10.1137/1011036.

[24] P. Wolfe, Convergence conditions for ascent methods. II: Some corrections, SIAM Rev. 13 (2) (1971) 185–188. doi:10.1137/1013035.

[25] J. D. Jansen, Adjoint-based optimization of multi-phase flow through porous media – a review, Computers & Fluids 46 (1) (2011) 40–51, 10th ICFD Conference Series on Numerical Methods for Fluid Dynamics (ICFD 2010). doi:10.1016/j.compfluid.2010.09.039.

[26] H. M. Nilsen, K.-A. Lie, O. Andersen, Fully-implicit simulation of vertical-equilibrium models with hysteresis and capillary fringe, Comput. Geosci. 20 (1) (2016) 49–67. doi:10.1007/s10596-015-9547-y.

[27] H. M. Nilsen, K.-A. Lie, O. Andersen, Robust simulation of sharp-interface models for fast estimation of CO2 trapping capacity, Comput. Geosci. 20 (1) (2016) 93–113. doi:10.1007/s10596-015-9549-9.

[28] O. Andersen, H. M. Nilsen, K.-A. Lie, Reexamining CO2 storage capacity and utilization of the Utsira Formation, in: ECMOR XIV – 14th European Conference on the Mathematics of Oil Recovery, Catania, Sicily, Italy, 8-11 September, EAGE, 2014. doi:10.3997/2214-4609.20141809.

[29] H. M. Nilsen, K.-A. Lie, O. Andersen, Analysis of CO2 trapping capacities and long-term migration for geological formations in the Norwegian North Sea using MRST-co2lab, Computers & Geosciences 79 (2015) 15–26. doi:10.1016/j.cageo.2015.03.001.

[30] O. Andersen, K.-A. Lie, H. M. Nilsen, An open-source toolchain for simulation and optimization of aquifer-wide CO2 storage, Energy Procedia 86 (2016) 324–333. doi:10.1016/j.egypro.2016.01.033.

[31] R. Allen, H. M. Nilsen, O. Andersen, K.-A. Lie, On obtaining optimal well rates and placment for CO2 storage, in: ECMOR XV – 15th European Conference on the Mathematics of Oil Recovery, Amsterdam, Netherlands, 29 August – 1 September, EAGE, 2016. doi:10.3997/2214-4609.201601823.

[32] R. Allen, H. M. Nilsen, O. Andersen, K.-A. Lie, Categorization of Norwegian Continental Shelf formations in terms of geological CO2 storage potentials, in: GHGT-13 – 13th International Conference on Greenhouse Gas Control, Lausanne, Switzerland, 14 – 18 November 2016, Energy Procedia, 2017.

[33] Usman, P. I. Utomo, Sugihardjo, L. S. Herru, A Systematic Approach to Source-Sink Matching for CO2 EOR and Sequestration in South Sumatera, Energy Procedia 63 (2014) 7750–7760. doi:10.1016/j.egypro.2014.11.809.

[34] M. Carpenter, A new offshore CO2 storage site in Norway, The FIRST SPE Norway magazine Winter (2017) 50–51, http://connect.spe.org/oslo/thefirst.

[35] L. Bjerge, Norcem CO2 capture project, Talk presented at International CCS Conference, 20–21 May, 2015, norcem.no/en/system/files_force/assets/document/6d/3c/4_-_liv_bjerge_-_norcem_co2_capture_project.pdf?download=1 (2015).

[36] Zero Emission Resource Organisation, Yara CCS project, zeroco2.no/projects/yara-ccs-project.

[37] Bellona Europa, Opening in oslo: A world first for CCS, bellona.org/news/ccs/2016-01-opening-in-oslo-world-first-within-ccs.

[38] Google maps 2017, accessed 2017-01-15.
URL maps.google.com

[39] M. L. Szulczewski, C. W. MacMinn, R. Juanes, Theoretical analysis of how pressure buildup and CO2 migration can both constrain storage capacity in deep saline aquifers, International Journal of Greenhouse Gas Control 23 (2014) 113–118. doi:10.1016/j.ijggc.2014.02.006.

[40] T. H. V. Pham, T. E. Maast, H. Hellevang, P. Aagaard, Numerical modeling including hysteresis properties for CO2 storage in Tubåen formation, Snøhvit field, Barents Sea, Energy Procedia 4 (2011) 3746–3753. doi:10.1016/j.egypro.2011.02.308.

[41] E. Lundin, S. Polak, R. Bøe, P. Zweigel, E. Lindberg, NGU Report 2005.027: Storage potential for CO2 in the Froan Basin area of the Trøndelag Platform, Mid-Norway, Tech. rep., Geological Survey of Norway / SINTEF, Trondheim (2005).

[42] V. Singh, A. Cavanagh, H. Hansen, B. Nazarian, M. Iding, P. Ringrose, Reservoir Modeling of CO2 Plume Behavior Calibrated Against Monitoring Data From Sleipner, Norway, in: SPE Annual Technical Conference and Exhibition, Florence, Italy, 2010. doi:10.2118/134891-MS.